Preparation of biomedical Ag incorporated hydroxyapatite/titania coatings on Ti6Al4V alloy by plasma electrolytic oxidation*

Zhou Lan(周 澜)[a)b)c)†], Lü Guo-Hua(吕国华)[c)‡], Mao Fei-Fei(毛菲菲)[d)], and Yang Si-Ze(杨思泽)[c)e)]

[a)] College of Mathematics & Physics, Nanjing University of Posts and Telecommunications, Nanjing 210003, China
[b)] Key Lab of Broadband Wireless Communication and Sensor Network Technology, Nanjing University of Posts and Telecommunications, Ministry of Education, Nanjing 210003, China
[c)] Institute of Physics, Chinese Academy of Sciences, Beijing 100190, China
[d)] Department of Oral and Maxillofacial Surgery, Interdisciplinary Laboratory, Peking University School of Stomatology, Beijing 100081, China
[e)] Fujian Key Laboratory for Plasma and Magnetic Resonance, Department of Aeronautics, School of Physics and Mechanical & Electrical Engineering, Xiamen University, Xiamen 361005, China

(Received 20 September 2013; revised manuscript received 5 November 2013; published online 14 January 2014)

Nano-Ag incorporated hydroxyapatite/titania (HA/TiO_2) coatings were deposited on Ti6Al4V substrates by the plasma electrolytic oxidation process. Compared with the substrate, the deposited coatings display attractive mechanical and biomedical properties. First, the coatings have stronger wear resistance and corrosion resistance. Second, they show a strong antibacterial ability. The mean vitality of the P. gingivalis on the coating surfaces is reduced to about 21%. Third, the coatings have good biocompatibility. The mean viability of the fibroblast cells on the coating surface is increased to about 130%. With these attractive properties, Ag incorporated HA/TiO_2 coatings may be useful in the biomedical field.

Keywords: hydroxyapatite, corrosion resistance, antibacterial ability, biocompatibility

PACS: 52.80.Wq, 68.55.Nq **DOI:** 10.1088/1674-1056/23/3/035205

1. Introduction

Ti6Al4V is an important implant material in orthopedic and dental fields. It has lots of attractive properties, such as high specific strength, high calorific intensity, low density, and low fracture toughness.[1] However, Ti6Al4V still has some defects in its practical application. First, it cannot form a chemical bond with bone tissue in the humoral environment, which may cause the formation of thrombus on the interface. Second, the corrosion resistance of Ti6Al4V is not good enough to avoid contact corrosion on the tissue–Ti6Al4V interface, which may lead to the corrosion damage of the implant device.[2,3] Moreover, Ti6Al4V has a poor antibacterial ability. As an implant material, bacterial infection after the placement is one of the potentially devastating complications, which may eventually cause the total failure of the implantation. Once bacterial infections occur on the tissue–implant interface, bacteria tend to aggregate in a hydrated polymeric matrix to form a bio-film on the implant device surface, which can hardly be destroyed by any antibacterial agents coming from outside.[4–6] Therefore, to promote its application in the biomedical field, the corrosion resistance, biocompatibility, and antibacterial activity of Ti6Al4V all need to be improved.[7–12]

Among various surface strategies, depositing a biofunctional coating on the surface of Ti6Al4V is a successful approach. Hydroxyapatite (HA) is a popular biomaterial in the medical field. As a component of bone, HA has good biocompatibility, osteoconductivity, and bioactivity.[13–15] Meanwhile, it can enhance early bone apposition and implant fixation.[16–18] However, the lattice of HA is quite different from that of metals, so it is quite difficult for the HA coating to chemically bond to the metal surfaces by conventional film deposition methods. Recently, the plasma electrolytic oxidation (PEO) technique has become a prominent way for depositing HA coatings on metal surfaces.[13–15,19–21] The coatings deposited by the PEO technique are usually characterized by interconnected microporous morphologies and multiphase structures. The PEO technique has a complex process. It combines the diffusion and electrophoresis of elements in the electrolyte, the transformation of ions in the discharge channels, and the electrochemical oxidation on the metal surface. Meanwhile, as the coating formation involves some consumption (oxidation) of the metal substrate, the deposited coating can adhere to the substrate firmly.[20–22] Especially, in the PEO process of the

*Project supported by the Young Scientists Fund of the National Natural Science Foundation of China (Grant No. 11005151), the National Natural Science Foundation of China (Grant No. 11347110), the Open Research Fund of the Key Lab of Broadband Wireless Communication and Sensor Network Technology of Ministry of Education, Nanjing University of Posts and Telecommunications, China (Grant No. NYKL201303), the Scientific Research Foundation of Nanjing University of Posts and Telecommunications, China (Grant No. NY213054), and the Priority Academic Program Development of Jiangsu Higher Education Institutions, China.

†Corresponding author. E-mail: zhoul@njupt.edu.cn
‡Corresponding author. E-mail: lvguohua@aphy.iphy.ac.cn

© 2014 Chinese Physical Society and IOP Publishing Ltd

Ti6Al4V substrate, the generated titanium oxide (TiO_2) inner layer can enhance the bonding strength between the coating and the substrate. Moreover, the dense TiO_2 layer shows good mechanical properties, such as strong corrosion resistance and wear resistance.[15] Therefore, depositing HA-contained coatings on the Ti6Al4V surface by the PEO technique may improve both the mechanical and the bioactivity of the Ti6Al4V substrate. However, the antibacterial ability of HA-contained coating is unclear. Worse still, as the PEO process makes the coating surface rougher, it may leave the sample at a higher risk of bacterial accumulation.[23–26] It is well known that silver (Ag) and its compounds are good antibacterial agents with a broad spectrum of activity.[27] They can prevent bacteria from replicating and finally inactivate the bacterial proteins. During the past decades, Ag and its compounds have been incorporated into the surfaces of various medical devices, such as the vascular, urinary, prosthetic heart valve sewing rings, sutures, fracture fixation, and so on.[28–33]

Based on the discussion above, depositing the nano-Ag incorporated HA-contained coating on the surface of Ti6Al4V may be an effective modification, which can improve its corrosion resistance, bioactivity, and antibacterial ability simultaneously. In this study, we deposit the nano-Ag incorporated HA-contained coating on the surface of a Ti6Al4V substrate by the PEO technique. To investigate the application potential of the deposited coating in the biomedical field, the mechanical and biomedical properties, such as the wear resistance, corrosion resistance, antibacterial ability, and biocompatibility are carefully studied.

2. Experimental details

2.1. Substrate preparation

A Ti6Al4V alloy with dimensions of 10 mm × 10 mm × 2 mm was used as the substrate. All the substrates were progressively polished with SiC abrasive papers (300–2000 ♯), then ultrasonically washed in acetone, absolute ethyl alcohol, and distilled water successively for 10 min to wipe off the contamination on the surface. After that, the substrates were dried at room temperature and kept in the sample box prior to the PEO treatment.

2.2. PEO process

The schematic diagram of the experimental setup is shown in Fig. 1. The PEO process was carried out in a conventional plasma electrolytic oxidation unit comprised of a pulsed DC source, a stirring system, and a cooling system. Based on the research results of Han *et al*,[34,35] we chose an aqueous electrolyte containing β-glycerophosphate disodium (β-$GPNa_2$) and calcium acetate ($Ca(CH_3COO)_2{\cdot}H_2O$) with the concentrations of 0.02 mol/L and 0.2 mol/L, respectively. To introduce nano-Ag in the deposited coatings, we added different amounts of nano-Ag solution (nano-Ag size: 10 nm) in the electrolyte. As shown in Table 1, the electrolytes without nano-Ag, with 50 mg/L nano-Ag, and with 5 mg/L nano-Ag are named electrolyte-1, electrolyte-2, and electrolyte-3, respectively. The coatings fabricated with the three electrolytes are named coating-1, coating-2, and coating-3, respectively. In the PEO process, the Ti6Al4V plate was used as the anode and the stainless steel stirrer was used as the cathode. The pulse frequency and duty ration of the power source were fixed at 1000 Hz and 10%, respectively. Our results have shown that under the above pulse frequency and duty ration, the deposited coatings have high density and strong corrosion resistance. The samples were treated with a constant current density of 8 A/dm^2 for 3 min. During the whole experiment process, the electrolyte was cooled with water at 3 °C provided by a cooling water circulate machine (BTY-CW-300). The final voltages at the end of the 3 min PEO process in the three electrolytes were 403 ± 3 V, 385 ± 2 V, and 387 ± 3 V, respectively. It is obvious that the addition of nano-Ag could reduce the final voltage.

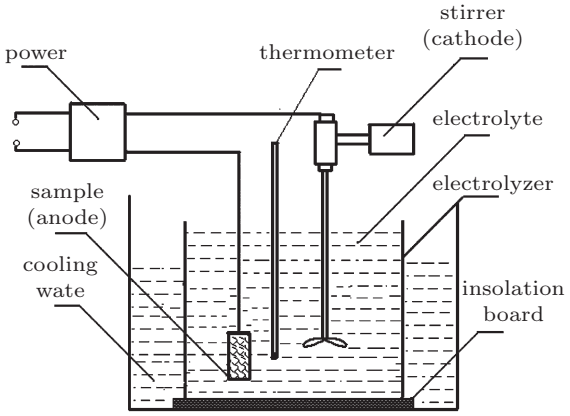


Fig. 1. Schematic diagram of experimental setup.

Table 1. Components of the electrolytes and the final voltages at the end of the PEO processes.

Electrolyte	β-$GPNa_2$ /(mol/L)	$Ca(CH_3COO)_2$ /(mol/L)	Nano-Ag /(mg/L)	Final voltage /V
Electrolyte-1	0.02	0.2	0	403 ± 3
Electrolyte-2	0.02	0.2	50	385 ± 2
Electrolyte-3	0.02	0.2	5	387 ± 3

2.3. Microstructure and surface characterization

The crystal structure of the PEO coatings was evaluated by using the diffraction patterns recorded with a D/max-2400 X-ray diffractometer (XRD, Cu Kα radiation, $\lambda = 0.154$ nm). The diffraction patterns were obtained between the 2θ values of 20° and 60° with a scanning speed of 2 °/min. The surface topography of the deposited coatings was detected

by a scanning electron microscope (SEM, HITACHI S-4200, Japan). The samples were sputter-coated with a thin layer of gold prior to the measurement. The elemental compositions of the deposited coatings were detected by an energy dispersive spectrometer (EDS) included in the SEM. The tribological behaviors of the deposited coatings were studied by dry friction tests, which were carried out on a ball-on-plate tribometer (Center for Tribology, HIT, China) with a normal load of 2 N. The rotation diameter of the test was 5 mm and the rotation speed was 200 r/min. The whole friction test for each sample lasted 5 min. During the test, the ambient temperature was 20 ± 2 °C and the relative humidity was 30%–45%. The corrosion resistance of the sample in the Hanks solution was detected by the potentiodynamic polarization measurements. The Hanks solution is a common balanced salt solution, which is usually used for culturing cells and tissues. The chemical compositions of the Hanks solution include NaCl: 136.9 mmol/L, KCl: 5.4 mmol/L, $MgSO_4 \cdot 7H_2O$: 0.8 mmol/L, $CaCl_2 \cdot 2H_2O$: 1.3 mmol/L, $Na_2HPO_4 \cdot 2H_2O$: 0.3 mmol/L, KH_2PO_4: 0.4 mmol/L, $NaHCO_3$: 4.2 mmol/L, and $C_6H_{12}O_6 \cdot H_2O$: 5 mmol/L. The potentiodynamic polarization test was carried out in the conventional three-electrode mode. The working electrode was the coated Ti6Al4V sample of interest, the counter electrode was a platinum sheet electrode, and the reference electrode was a saturated calomel electrode (SCE, Aldrich Chemical). Before the polarization test, all the samples were kept in the Hanks solution for 30 min to obtain a steady measurement value. During the test process, the temperature of the Hanks solution was kept at 37 °C to simulate human body temperature. The scan rate was fixed at 0.5 mV/s and the whole polarization test for each sample lasted about 30 min. CorrView 2.90 (Scribner Associates. Inc., USA) was used for data acquisition and analysis. The reported data were the mean values of at least three reproducible measurements.

2.4. Short-term bacterial adhesion experiment

The antibacterial ability of the deposited coatings was tested in a short-term bacterial adhesion experiment. In our experiment, P. gingivalis was used as the tested bacteria. Prior to the experiment, P. gingivalis was cultured in the brain heart infusion (BHI) in the anaerobic environment (80% N_2, 10% CO_2, and 10% H_2) at 37 °C for 48 h. The short-term bacterial adhesion experiment was performed in a Microbial Viability Assay Kit-WST Kit (Japan), whose working solution contained water-soluble tetrazolium (WST-8) and dimethyl sulfoxide (DMSO) (WST-8:DMSO=9:1). With the help of the electron carrier, the dehydrogenase from the micro-organisms can reduce the WST-8 into highly water-soluble formazan dyes and the amount of the formazan is proportional to the amount of micro-organisms. Making use of this proportional relation, the amount of micro-organisms can be detected. In the experiment, the uncoated and coated Ti6Al4V samples were sterilized under UV irradiation for 30 min and located in the test tube with 720 μL BHI. The P. gingivalis suspension was diluted by the sterilized phosphate buffered saline (PBS) to make its absorbance (OD) at 550 nm reach 0.125. Then, the suspension was further diluted until the P. gingivalis was at a concentration of 1×10^7 cfu/ml. Next, 40 μL P. gingivalis suspension was put into every test tube with the test sample, and incubated for 6 h. After that, the samples were removed from the tubes and washed with PBS three times. Next, each sample was located in the test tube with 180 μL new BHI and 10 μL working solution, and further incubated for 2 h. Finally, the samples were removed from the test tubes, and the OD value of the solution at 450 nm in each test tube was measured by a microplate reader. The mean bacterial vitality can be calculated according to the formula

$$\text{bacterial vitality}\ (\%) = \frac{\text{OD}_\text{E} - \text{OD}_\text{B}}{\text{OD}_\text{C} - \text{OD}_\text{B}} \times 100\%, \qquad (1)$$

where OD_E, OD_B, and OD_C represent the OD values of the experimental group, the blank group, and the control group, respectively.

To investigate the morphology of the P. gingivalis attached on the sample surface, 10 μL P. gingivalis suspension at a concentration of 1×10^7 cfu/ml was seeded on the surfaces of the samples. Then, the samples were located in the test tube with 190 μL BHI, and cultured in a CO_2 incubator for 24 h. After that, the samples were washed with PBS, and the P. gingivalis attached on the surfaces were fixed with glutaraldehyde for 1 h. Sequentially, the P. gingivalis were gradiently dehydrated with the ethanol (30%, 50%, 70%, 80%, 90%, 95%, and 100%) and dried in a vacuum.

2.5. Cell adhesion experiment

The mouse fibroblast cell (L929) adhesion experiment was performed to study the biocompatibility of the samples. Prior to the experiment, the mouse fibroblast cells were cultured in an incubator at 37 °C in an atmosphere of 5% CO_2 and saturated humidity. The culture medium was the Dulbecco's modified Eagle's medium (DMEM, Sigma) with 10% foetal bovine serum (FBS, Sigma) and 1% penicillin-streptomycin antibiotic (Sigma). Non-adherent cells were removed by changing the medium every 24 h. When the coverage reached 80%–90%, the culture dishes were washed by the PBS, and digested by 0.25% trypsin-EDTA (Gibco) for 2–3 min. Then, the cell suspensions were centrifuged for 5 min (1000 rpm/min) and subcultured. Cells subcultured after 3–7 passages were used in the cell adhesion experiments. The cell viability was detected by the CCK-8 measurement. The basic principle for detecting the mean cell viability is quite similar

to that of the mean bacterial vitality. In the experiment, the samples were sterilized under UV irradiation for 30 min and located in a 96-well plate. The cell suspension at a concentration of 4×10^4 mL^{-1} was seeded on the surfaces of the samples and cultured in a CO_2 incubator at 37 °C for 4 h. After that, the samples were removed from the tubes and located in a new 96-well plate with 100 μL DMEM and 10 μL CCK-8. After being cultured in the CO_2 incubator at 37 °C for 4 h, the cell suspension was sucked out and its OD value at 450 nm was measured by a microplate reader. The mean cell viability can also be calculated based on Eq. (1).

To investigate the morphology of the L929 cells attached on the samples, the cell suspension at a concentration of 4×10^4 mL^{-1} was seeded on the sample surface, and cultured in the CO_2 incubator at 37 °C for 24 h. Then, the sample was washed with the PBS and fixed with 2.5% glutaraldehyde for 1 h. Sequentially, the L929 cells were gradiently dehydrated with the ethanol (30%, 50%, 70%, 80%, 90%, 95%, and 100%) and dried in the vacuum.

3. Results and discussion

3.1. Crystal structure, morphology, and element composition of the deposited coatings

The XRD patterns of the Ti6Al4V substrate and the three deposited coatings are shown in Fig. 2. It can be seen in Figs. 2(ii)–2(iv) that the intensities of the substrate peaks are greatly reduced, this is because the substrate surfaces are covered by the dense coatings. In the three coatings, the titanium oxides primarily are in the rutile phase. Moreover, HA peaks can be detected in all three coatings, which indicates that the HA-like coatings are formed in the experiment. Based on the research in Refs. [36]–[41], the micro-discharges develop and extinguish rapidly (within 10^{-4} to 10^{-5} s) in the vicinity of the anode in the PEO process. The discharge can heat the metal substrate to about 373–423 K. Meanwhile, the local temperature and pressure inside the discharge channels can reach 10^3–10^4 K and 10^2–10^3 MPa, respectively. The extremely high temperature and pressure may lead to plasma thermochemical interactions between the substrate and the electrolyte, which results in the formation of metal-quenched oxides and complex compounds on the substrate surface. It is well known that titanium dioxide crystallizes mainly in two forms, anatase and rutile phases. In the PEO process, the rutile phase increases steadily with the increase of the applied voltage, while the anatase phase increases first and then decreases with the increase of the applied voltage.[38,39] In our experiment, a relatively high voltage was used (about 400 V) to fabricate the HA-like coatings. Such a high applied voltage could warm the anode up, as more electrical sparks appeared in the vicinity of the anode. With this extra heat, the anatase phase, which is a meta-stable phase, can transform to the thermodynamically stable rutile phase. Therefore, we did not detect any anatase peak in the XRD patterns. On the other hand, for coating-2 and coating-3 (Figs. 2(iii) and 2(iv)), no feature peaks of Ag-contained compounds were detected, which indicates that the incorporation of a trace amount of nano-Ag in the electrolyte has almost no effect on the phase compositions of the deposited coating.

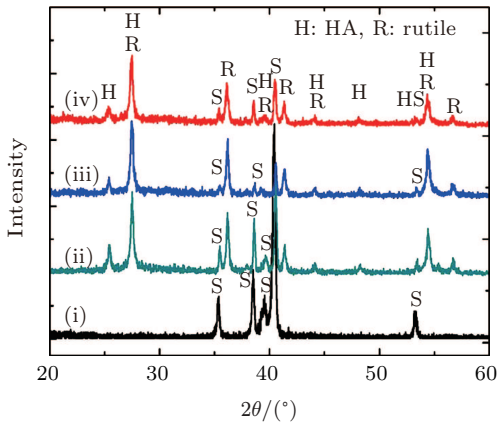


Fig. 2. (color online) XRD patterns of the Ti6Al4V substrate and the coatings fabricated with the three electrolytes: (i) Ti6Al4V substrate, (ii) coating-1, (iii) coating-2, (iv) coating-3.

Figure 3 illustrates the surface features of the three coatings with the magnifications of 1000 (main plot) and 6000 (inset). All the three coatings show the typical surface morphology of the ceramic coatings fabricated in the PEO process, which possesses a porous characteristic with some volcano top-like pores distributed randomly. The generation of the porous surface can be explained as follows. During the PEO process, a large number of visible sparks occur when the applied voltage exceeds the critical voltage for the barrier layer breakdown. When a spark extinguishes, the melted substances will erupt from the discharge channel, which can leave a crater-like hole in the coating surface.[38,42] Meanwhile, there are some cracks in the coating surfaces. The cracks are formed by the internal stress, which comes from the constant effect of the plasma discharge on the coating surface.[43] On the other hand, it can be found that the introduction of a trace amount of nano-Ag in the electrolyte can slightly reduce the micropore diameter of the deposited coatings. The micropore diameter of coating-1 is about 5 μm (Fig. 3(a)), while those of coating-2 and coating-3 (Figs. 3(b) and 3(c)) are about 2–3 μm. It is known that the micropore diameter of the deposited coatings will increase with the increase of the applied voltage.[38,39] In Section 2, we have shown that the addition of nano-Ag in the electrolyte can slightly reduce the final voltage of the PEO precess, so it can reduce the micropore diameter of the deposited coatings.

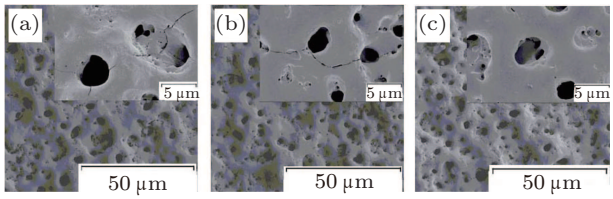


Fig. 3. (color online) SEM photographs of the HA-like coatings fabricated with the three electrolytes: (a) coating-1, (b) coating-2, (c) coating-3. The magnification is 1000 in the main figure and 6000 in the inset.

The element compositions of the three HA-like coatings are shown in Table 2. It can be found that there are six elements in the coatings. Ti, V, and Al come from the substrate, while elements Ca, P, and O are introduced by the PEO process. Ca, P, and O are the major elements of the HA, so the EDS result is consistent with the XRD result. The contents of the six elements in the three coatings are quite similar. The small variation of the main elements can be attributed to two factors. First, the EDS measurement has a systematic error. Second, the applied voltages for the three deposited coatings are slightly different, which leads to the variation of the element composition. On the other hand, the Ag element is not detected in coating-2 and coating-3. It is speculated that as the contents of nano-Ag in electrolyte-2 and electrolyte-3 are extremely low (50 mg/L and 5 mg/L), the Ag content in the deposited coating is below the detection limit of EDS measurement (0.1 wt.%).

Table 2. Elemental compositions (wt.%) of the three HA-like coatings.

Sample	Ti	O	Ca	P	Al	V
Coating-1	40.87	43.83	7.70	3.18	2.35	2.07
Coating-2	41.37	42.68	8.22	3.44	2.43	1.86
Coating-3	40.53	44.59	7.49	3.38	1.98	2.03

3.2. Wear resistance of the three deposited coatings

The wear resistance is an important property for an implant material. The coefficients of friction (COFs) of the three HA-like coatings are shown in Fig. 4. The COF for uncoated Ti6Al4V (0.3653 ± 0.0135) is used for comparison. The COF of the Ag free HA-like coating (coating-1) is 0.6035 ± 0.0126, which is obviously higher than that of the Ti6Al4V substrate. It indicates that the wear resistance of the Ag free HA-like coating is lower than the Ti6Al4V substrate. Meanwhile, the incorporation of Ag can effectively reduce the COF of the deposited coatings. The COFs of coating-2 and coating-3 are 0.2611 ± 0.0201 and 0.3141 ± 0.0179, respectively, even slightly lower than that of the Ti6Al4V substrate. It indicates that by depositing the Ag incorporated HA-like coating on the surface, the wear resistance of the Ti6Al4V substrate can be slightly improved.

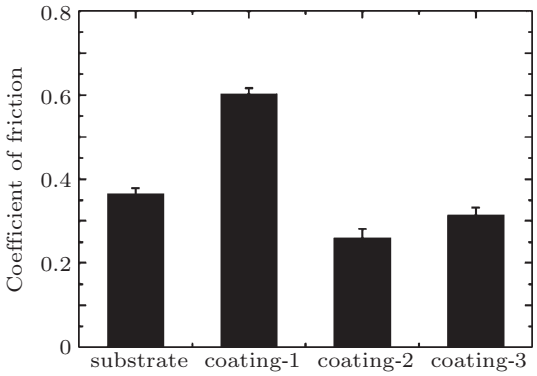


Fig. 4. Coefficients of friction of the Ti6Al4V substrate and three deposited coatings.

3.3. Corrosion resistance of the three deposited HA-like coatings

The potentiodynamic measurement results and the corresponding fitting parameters obtained by CorrView software are given in Fig. 5 and Table 3, respectively. The curve of the uncoated Ti6Al4V substrate is shown for comparison (Fig. 5(i)). By the PEO process, the corrosion potential (E_{corr}) of the sample (-455 ± 3 mV/SCE) increases greatly (coating-1: -8 ± 2 mV/SCE, coating-2: -40 ± 3 mV/SCE, coating-3: -24 ± 3 mV/SCE), which indicates that a better corrosion protection can be obtained. Meanwhile, it can be found that the Ag incorporation can slightly reduce the corrosion potential of the deposited coating, which indicates that the incorporation of Ag slightly reduces the corrosion resistance of the deposited coating. On the other hand, by depositing the HA-like coatings on the surface, the corrosion current density (I_{corr}) of the Ti6Al4V sample (0.05 μA/cm^2) is reduced by one order of magnitude (coating-1: 0.003 μA/cm^2, coating-2: 0.002 μA/cm^2, coating-3: 0.005 μA/cm^2). It is well known that the corrosion rate is normally proportional to I_{corr}. The lower the I_{corr}, the lower the corrosion rate.[44,45] Therefore, by depositing the HA-like coatings on the surfaces, the corrosion rate of the Ti6Al4V sample in the Hanks solution can be greatly reduced. By comparing the three coatings, it can be found that although the incorporation of nano-Ag in the electrolyte can slightly reduce the corrosion voltage, it almost has no effect on the corrosion current density. Therefore, the Ag incorporation only has a slight weakening effect on the corrosion resistance of the deposited coating.

Table 3. Electrochemical polarization parameters of the Ti6Al4V substrate and the three deposited coatings in the Hanks solution at 37 °C.

Sample	E_{corr} /(mV, SCE)	I_{corr} /(μA/cm^2)	β_a /(mV/decade)	β_c /(mV/decade)
Substrate	-455 ± 3	0.05 ± 0.001	485 ± 16	133 ± 20
Coating-1	-8 ± 2	0.003 ± 0.0006	110 ± 15	96 ± 10
Coating-2	-40 ± 3	0.002 ± 0.001	160 ± 18	427 ± 12
Coating-3	-24 ± 3	0.005 ± 0.001	185 ± 15	257 ± 16

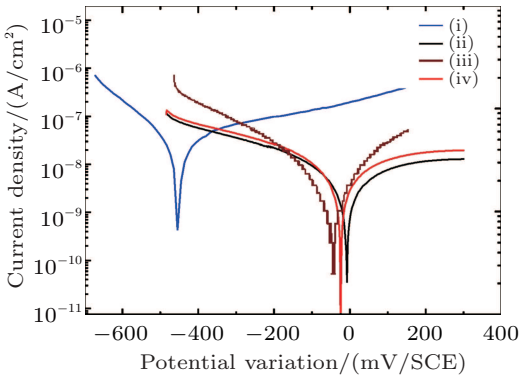


Fig. 5. (color online) Potentiodynamic polarization curves of the Ti6Al4V substrate and the three deposited coatings in the 37 °C Hanks solution: (i) Ti6Al4V substrate, (ii) coating-1, (iii) coating-2, (iv) coating-3.

3.4. Antibacterial activity and the biocompatibility of the three HA-like coatings

The morphologies of the P. gingivalis attached on the three HA-like coatings with a magnification of 4000 are shown in Fig. 6. As is shown in Fig. 6(a), the P. gingivalis attached on coating-1 is spherical shaped with a smooth surface. Especially, some are split without damage. However, the morphologies of the P. gingivalis on coating-2 and coating-3 (Figs. 6(b) and 6(c)) are quite different. It is obvious that the cytoplasm membranes of the P. gingivalis on the coating surface shrink. The vitalities of the P. gingivalis are shown in Fig. 7. The mean vitality of the P. gingivalis attached on the uncoated Ti6Al4V substrate is shown for comparison. It is clear that the vitality of the P. gingivalis on coating-1 is $(96.6 \pm 2.2)\%$, which is extremely close to that of the Ti6Al4V substrate. It indicates that the Ag-free HA-like coating has no antibacterial activity. However, the vitality of the P. gingivalis on coating-2 and coating-3 is largely reduced to about $(21.2 \pm 3.2)\%$ and $(31.8 \pm 4.1)\%$, respectively. The bacterial behavior experiment proves that the incorporation of a trace amount of nano-Ag in the electrolyte can greatly improve the antibacterial activity of the deposited coatings. Moreover, it can be found that coating-2 fabricated in the electrolyte with a higher Ag content shows stronger antibacterial activity.

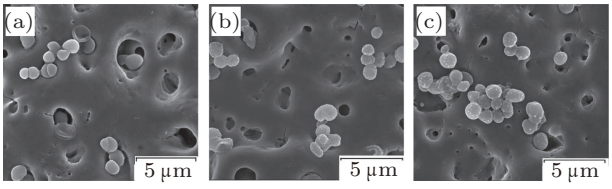


Fig. 6. SEM morphologies of the P. gingivalis attached on the three HA-like coatings with a magnification of 4000: (a) coating-1, (b) coating-2, (c) coating-3.

Research by Shirkhanzadeh and Azadegan[46] has shown that the nano-Ag atom can interact with the water and release Ag^+. During the PEO process, the Ag^+ can be incorporated into the HA crystal structure via the dissolution–precipitation and ion-exchange mechanisms. Ag^+ can locate in the HA crystal structure, or may bind to phosphate ions to form nanoclusters of silver phosphate, which uniformly disperse on the HA crystals. In this way, the Ag levels in the deposited coating can be engineered by increasing or reducing the Ag content in the electrolyte.[47] In practical antibacterial applications, the Ag atoms and Ag^+ can be slowly released from the coating surface at a bactericidal concentration. So far, the antibacterial ability of Ag has not been fully understood. The research in Ref. [48] showed that when the nano-Ag particles are small and release a large amount of Ag^+, the antibacterial activity is dominated by the Ag^+. The Ag^+ may combine with sulfhydryl groups of the respiratory enzyme or the nucleic acids in bacteria, which can finally lead to blocking the breathing and cause the death of the bacteria. Feng *et al* once reported that the Ag^+ can penetrate the cell membrane and enter the cells, subsequently turn DNA into a condensed form and make the DNA lose replication abilities. Meanwhile, the Ag^+ can interact with the thiol groups in protein, which also may lead to the inactivation of the bacterial proteins.[49]

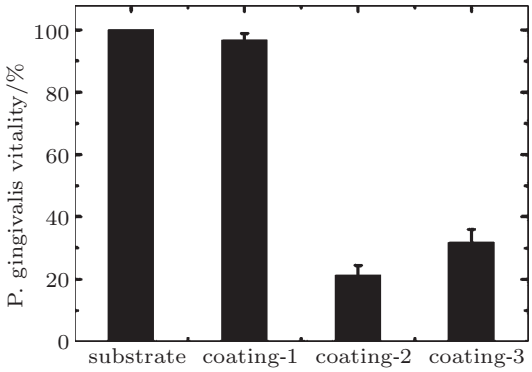


Fig. 7. Mean vitalities of the P. gingivalis attached on the Ti6Al4V substrate and three HA-like coatings.

The morphologies of the mouse fibroblast cells attached on the HA-like coatings with a magnification of 1000 are shown in Fig. 8. It can be found that the fibroblast cells accommodate conformably onto the coating surface, and the filopodia and unidirectional lamellipodia extensions are apparent. No obvious difference of the cell morphologies on the three coatings can be observed. The mean viabilities of the mouse fibroblast cells on the substrate and the three HA-like coatings are shown in Fig. 9. It is obvious that the cell viability on each of the three coatings is higher than that on the Ti6Al4V substrate (coating-1: $(131.32 \pm 5.5)\%$, coating-2: $(127.17 \pm 4)\%$, coating-3: $(136.03 \pm 4.2)\%$), which indicates that the three HA-like coatings show better biocompatibility than the Ti6Al4V substrate. This is because the HA is a component of bone and the deposited HA-like coatings have better biocompatibility and bioactivity than the Ti6Al4V substrate. Meanwhile, it can be found that the incorporation of nano-Ag

causes little influence on the biocompatibility of the deposited coating. During the past few years, some researchers have discussed the merit and demerit effects of the Ag incorporation in the bioperformance of the HA coatings.[50–53] The merit effect includes that it can enhance the antibacterial ability of the coatings, while the demerit is that it may reduce the cell viability and activity. In 2008, Chao *et al* showed that decreasing the Ag content can improve the biocompatibility of the Ag incorporated coatings largely. They also proved that the nano-Ag incorporated HA coatings with $< 5\%$ Ag content has no cytotoxicity to the cells.[54] Combined with the elemental composition results, in our experiment, the Ag contents in coating-2 and coating-3 are far less than 5%, so both the Ag incorporated coatings have no cytotoxicity.

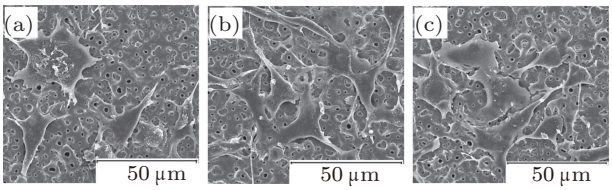


Fig. 8. SEM morphologies of the mouse fibroblast cells attached on the three coatings at the magnification of 1000: (a) coating-1, (b) coating-2, (c) coating-3.

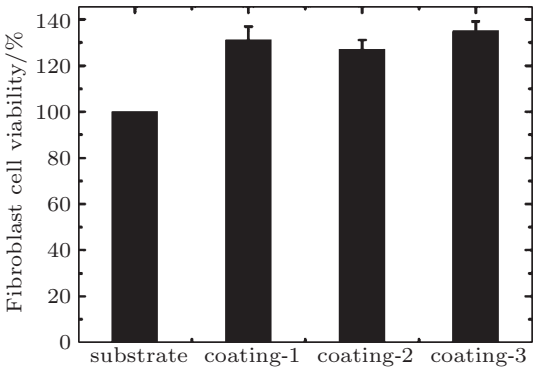


Fig. 9. The mean viabilities of the mouse fibroblast cells attached on the substrate and the three deposited coatings.

4. Conclusion

In the paper, we successfully deposit nano-Ag incorporated HA-like coatings on the Ti6Al4V substrates by the PEO technique. The coatings display the typical porous surface morphology. As the addition of nano-Ag in the electrolyte can slightly reduce the final voltage, it can slightly reduce the micropores on the coating surface. The Ag incorporated HA-like coatings exhibit good mechanical properties. By depositing the coatings on the surface, the COF of the Ti6Al4V samples can be slightly reduced from 0.36 to 0.26 and 0.31, which shows that the wear resistance of the deposited coatings is slightly stronger than that of the substrate. Meanwhile, the corrosion voltage of the coated samples increases greatly from -455 mV/SCE to -40 mV/SCE and -24 mV/SCE, and the corrosion current density is reduced by one order of magnitude. The results indicate that the corrosion resistance of the coated samples can be greatly improved. Meanwhile, the Ag incorporated coatings exhibit good biomedical properties. First, as the Ag contents of the coatings are extremely low, the coatings have no cytotoxicity. Moreover, compared with the Ti6Al4V substrates, the mean viability of the mouse fibroblast cell attached on the coatings can reach about 130%, which indicates that the coatings have better biocompatiblity. Second, the coatings show strong antibacterial activity. The mean vitality of the P. gingivalis attached on the coating surfaces can be reduced to about 21% and 32%. Based on the good mechanical and biomedical properties, the nano-Ag incorporated HA-like coatings may be useful in the biomedical field.

Acknowledgment

The authors gratefully acknowledge the help of Professor Fu Zhi-Qiang from China University of Geosciences.

References

[1] Kasemo B and Prosthet J 1983 *Dent.* **49** 832
[2] Sennerby L, Thomsen P and Ericson L E 1992 *J. Mater. Sci: Mater. Med.* **3** 262
[3] Steflif D E, Sisk A L, Parr G R, Garner L K, Hanes P J, Lake F T, Berkery D J and Brewer P 1993 *J. Biomed. Mater. Res.* **27** 791
[4] Costerton J W, Stewart P S and Greenberg E P 1999 *Science* **284** 1318
[5] Nasser S 1992 *Orthop. Clin. North. Am.* **23** 265
[6] Hendriks J G E, van Horn J R, van der Mei H C and Busscher H J 2004 *Biomaterials* **25** 545
[7] Han Y, Hong S H and Xu K W 2003 *Surf. Coat. Technol.* **168** 249
[8] Sun X T, Jiang Z H, Xin S G and Yao Z P 2005 *Thin Solid Films* **471** 194
[9] Nie X, Leyland A and Matthews A 2000 *Surf. Coat. Technol.* **125** 407
[10] Gu J D and Chen P L 2006 *Surf. Coat. Technol.* **200** 3341
[11] Zhou L, Lv G H, Ji C and Yang S Z 2012 *Thin Solid Film* **520** 2505
[12] Zhou L, Lv G H, Pang H, Zhang G P and Yang S Z 2012 *Surf. Coat. Technol.* **206** 2552
[13] Wei D and Zhou Y 2009 *Ceram. Int.* **35** 2343
[14] Han J Y, Yu Z T and Zhou L 2008 *Appl. Surf. Sci.* **255** 455
[15] Qiu D, Yang L, Yin Y and Wang A 2011 *Surf. Coat. Technol.* **205** 3280
[16] Bauer T W, Geesink R G T, Zimmerman R and McMahon J T 1991 *J. Bone J. Surg.* **73** 1439
[17] Clemens J A M, Klein C P A T, Vriesde R C, Rozing P M and de Groot K 1998 *J. Biomed. Mater. Res.* **40** 341
[18] Dunn D S, Raghavan S and Volz R G 1993 *J. Biomed. Mater. Res.* **27** 895
[19] Chen H, Lv G H, Zhang G L, Pang H, Wang X Q, Lee H J and Yang S Z 2010 *Surf. Coat. Technol.* **205** S32
[20] Curran J A and Clyne T W 2006 *Acta Materialia* **54** 1985
[21] Curran J A and Clyne T W 2005 *Surf. Coat. Technol.* **199** 168
[22] Yerokhin A L, Nie X, Leyland A and Matthews A 2000 *Surf. Coat. Technol.* **130** 195
[23] Esposito M, Hirsch J M, Lekholm U and Thomsen P 1998 *Eur. J. Oral Sci.* **106** 721
[24] Kotharu V, Nagumothu R, Arumugam C B, Veerappan M, Sankaran S and Davoodbasha M 2012 *Ceram. Int.* **38** 731
[25] van de Belt H, Neut D, Schenk W, van Horn J R, van der Mei H C and Busscher H J 2001 *Acta Orthop.* **72** 557
[26] Shi Z, Neoh K G, Kang E T and Wang W 2006 *Biomaterials* **27** 2440
[27] Lansdown A B G, Williams A, Chandler S and Benfield S 2005 *J. Wound Care* **14** 155
[28] Bosetti M, Masse A, Tobin E and Cannas M 2002 *Biomaterials* **23** 887
[29] Grunlan J C, Choi J K and Lin A 2005 *Biomacromolecules* **6** 1149
[30] Ewald A, Gluckermann S K, Thull R and Gbureck U 2006 *Biomed. Eng. Online* **5** 22

[31] Saint S, Elmore J G, Sullivan S D, Emerson S S and Koepsell T D 1998 *Am. J. Med.* **105** 236
[32] Darouiche R O 1999 *Clin. Infect. Dis.* **29** 1371
[33] Alt V, Bechert T, Steinrucke P, Wagener M, Seidel P, Dingeldein E, Domann E and Schnettler R 2004 *Biomaterials* **25** 4383
[34] Sun J, Han Y and Huang X 2007 *Surf. Coat. Technol.* **201** 5655
[35] Han Y, Sun J F and Huang X 2008 *Electrochem. Commun.* **10** 510
[36] Van T B, Brown S D and Wirtz G P 1977 *J. Bull, Am. Ceram. Soc.* **56** 563
[37] Vijh A K 1971 *Corros. Sci.* **11** 411
[38] Yerokhin A L, Nie X, Leyland A, Matthews A and Dowey S J 1999 *Surf. Coat. Technol.* **122** 73
[39] Bayati M R, Moshfegh A Z and Golestani-Fard F 2010 *Electrochim. Acta* **55** 3093
[40] Lv G H, Chen H, Wang X Q, Pang H, Zhang G L, Zou B, Lee H J and Yang S Z 2010 *Chin. Phys. B* **19** 085202
[41] Zhang G L, Wang J L, Liu Y F, Liu C Z and Yang S Z 2004 *Chin. Phys. B* **13** 1309
[42] Tang H, Sun Q, Yi C G, Jiang Z H and Wang F P 2012 *J. Mater. Sci.* **47** 2162
[43] Wang Z J, Wu L N, Cai W, A S and Jiang Z H 2010 *J. Alloys Compd.* **505** 188
[44] Angelini E, Grassini S, Rosalbino F, Fracassi F and d'Agostino R 2003 *Prog. Org. Coat.* **46** 107
[45] Creus J, Mazille H and Idrissi H 2000 *Surf. Coat. Technol.* **130** 224
[46] Shirkhanzadeh M and Azadegan M 1998 *J. Mater. Sci. Mater. Med.* **9** 385
[47] Ghani Y, Coathup M J, Hing K A and Blunn G W 2012 *J. Orthop. Res.* **30** 356
[48] Sotiriou G A and Pratsinis S E 2010 *Environ. Sci. Technol.* **44** 5649
[49] Feng Q L, Wu J, Chen G Q, Cui F Z, Kim T N and Kim J O 2000 *J. Biomed. Mater. Res.* **52** 662
[50] AshaRani P V, Low Kah Mun G, Hande M P and Valiyaveettil S 2009 *ACS Nano* **3** 279
[51] Cao X L, Cheng C, Ma Y L and Zhao C S 2010 *J. Mater. Sci. Mater. Med.* **21** 2861
[52] Watari F, Takashi N, Yokoyama A, Uo M, Akasaka T, Sato T, Abe S and Totsuka Tohji K 2009 *J. R. Soc. Interface* **6** 371
[53] Aillon K L, Xie Y, El-Gendy N, Berkland C J and Forrest M L 2009 *Adv. Drug. Deliv. Rev.* **61** 457
[54] Chen Y, Zheng X, Xie Y, Ding C, Ruan H and Fan C 2008 *J. Mater. Sci. Mater. Med.* **19** 3603